IEEE Access
Multidisciplinary | Rapid Review | Open Access Journal

Received July 28, 2020, accepted August 18, 2020, date of publication August 24, 2020, date of current version September 9, 2020.

Digital Object Identifier 10.1109/ACCESS.2020.3018906

Design of Low-Profile Dual-Band Printed Quadrifilar Helix Antenna With Wide Beamwidth for UAV GPS Applications

HONGMEI LIU[1], (Member, IEEE), MINGKE SHI[2], SHAOJUN FANG[1], (Member, IEEE), AND ZHONGBAO WANG[1], (Member, IEEE)

[1]School of Information Science and Technology, Dalian Maritime University, Dalian 116026, China
[2]Kunming Shipborne Equipment Research and Test Center, China State Shipbuilding Corporation Ltd., Kunming 650000, China

Corresponding author: Shaojun Fang (fangshj@dlmu.edu.cn)

This work was supported in part by the National Natural Science Foundation of China under Grant 51809030 and Grant 61871417 in part by the China Postdoctoral Science Foundation under Grant 2017M611210 in part by the Natural Science Foundation of Liaoning Province under Grant 2020-MS-127 and Grant 2019-MS-024 and in part by the Fundamental Research Funds for the Central Universities under Grant 3132020207 and Grant 3132020206.

ABSTRACT In the paper, a low-profile dual-band printed quadrifilar helix antenna (PQHA) with wide beamwidth is presented for UAV GPS applications. The antenna is composed of a hollow dielectric cylinder with four arms of dual-helix metal strips and a hollow dielectric ring with four pairs of circular metal strips. To provide dual-band operation, different lengths of the dual-helix metal strips are applied. By loading the circular metal strips on the dual-helix metal strips, size reduction of the antenna height is realized. Moreover, wide beamwidth is obtained. A miniaturized quad-feed network is also designed to provide equal amplitude signals with sequentially quadrature phases. To validate the proposed structure, a prototype is fabricated. The height of the antenna is 18.5 mm. The experimental results show that good impedance matching ($|S_{11}| < -18$ dB) and axial ratio (<2 dB) are obtained at GPS L1/ L2 bands. At 1.227 GHz, the measured 3-dB axial ratio beamwidths (ARBWs) are 186° and 187° at *xoz* and *yoz* planes, respectively. While the values are 167° and 163° at 1.575 GHz. The measured half-power beamwidths (HPBWs) are both more than 120° at the two bands. The results indicate that the proposed PQHA is a good candidate for UAV GPS applications.

INDEX TERMS Printed quadrifilar helix antenna (PQHA), dual band, GPS, wide beamwidth, miniaturization.

I. INTRODUCTION

Unmanned aerial vehicles (UAVs) are widely used for exploration, surveillance, data and multimedia communications, and telemetry applications. Recent advances in UAV-related technologies have led to an increasing demand of small, lightweight antennas for communication and navigation [1], [2]. During the operation of UAVs, the position information of the UAV can be obtained by GPS positioning. To receive signals from GPS orbiting satellites, the GPS antenna is required to have right-hand circular polarization (RHCP) and a uniform mode covering the entire upper hemisphere.

In previous researches on GPS antenna, the quadrifilar helix antennas (QHA) are well studied [3]–[6], which usually have good circular polarization (CP) performance. Improved from QHA, printed quadrifilar helix antennas (PQHA) are developed with four radiation elements printed on flexible dielectric substrate [7]–[10]. Generally, the PQHA is composed of four parallel helix-shaped quadrifilar radiation elements, and each radiating element is fed in phase quadrature at the endpoint close to the bottom ground.

Although the structure of PQHA is already small, further size reduction is required to meet the space limitations and the high overload for unmanned platform application. Several achievements to reduce antenna size have already been developed including inserting dielectric loading [11], [12], applying different helix turn angle [13], folding the helix antenna arms [14], using the impedance matching network [15] and the power divider networks [16]. Recently, methods for miniaturizing dual-band or triple-band antenna have also been proposed. In [17] and [18], dual-band PQHAs

The associate editor coordinating the review of this manuscript and approving it for publication was Venkata Ratnam Devanaboyina.

with stepped-width arms and dual-faced slot radiation structure are proposed. In [19], by meandering and turning the helix arms into the form of square spirals, size reduction of 43 % is obtained. More recently, a miniaturized dual-band spiral PQHA for UAV application is proposed by surface and inner dielectric loading [20]. Although the techniques described above would reduce the antenna's size, each of these techniques has some specific advantages and limitations with respect to impedance bandwidth, radiation pattern, size and structural strength. In GPS systems, the positioning needs receive signals from at least four satellites. Thus, CP antennas with 3-dB axial ratio beamwidth (ARBW) of larger than 120° and high gain at low elevations are more preferred for better reception of signals no matter whether the satellites are in low or high elevations. However, the features of wide 3-dB ARBW and high gain at low elevations are often ignored by most of the PQHAs.

In the paper, a low-profile dual-band PQHA with wide beamwidth is proposed for GPS L1/L2 applications. It consists of a hollow dielectric ring and a hollow cylinder with metal strips etched on the external surfaces. By loading the hollow dielectric ring on the hollow cylinder as the metal strip supporter, size reduction of the PQHA is realized. Moreover, the beamwidth is also broadened. For verification, a prototype is fabricated and measured. The experimental results show that the advantages of compact structure, good AR, broad beamwidth, high cross-polarization discrimination and low profile are exhibited by the proposed antenna. This paper is organized as follows. Section II presents the proposed PQHA. Section III introduces the implementations followed by a conclusion in Section IV.

II. DESIGN OF THE PROPOSED PQHA

A. ANTENNA CONFIGURATION

The structure of the proposed PQHA is shown in Figure 1. It is composed of a hollow dielectric supporting ring with four pairs of circular metal strips, a hollow dielectric supporting cylinder, a cylinder substrate etching by four pairs of dual-helix metal strips, four grounding lines, four feeding lines, a ground plane, and a quad-feed network. The hollow dielectric supporting ring and the hollow supporting cylinder are fabricated using 3-D printed technique with the material of nylon. The measured permittivity of the nylon is 3 in the experimental environment. The hollow dielectric supporting ring is mounted on the top of the hollow dielectric supporting cylinder. The F4B ($\varepsilon_r = 3.5$, $\tan\delta = 0.003$, $h = 0.2$ mm) is selected as the substrates for supporting the dual-helix metal strips and the feed network. In the design, a miniaturized quad-feed network is utilized to provide equal amplitude signals with sequentially quadrature phases. The feed network is composed of three Wilkinson power dividers, a 180° phase shifter, and two 90° phase shifters. Since the space is limited on the unmanned platform, the BP2G1+ chip working in the range of 1.2 GHz ∼ 2.0 GHz is utilized as the power divider for size reduction of the feed network. Modified phase

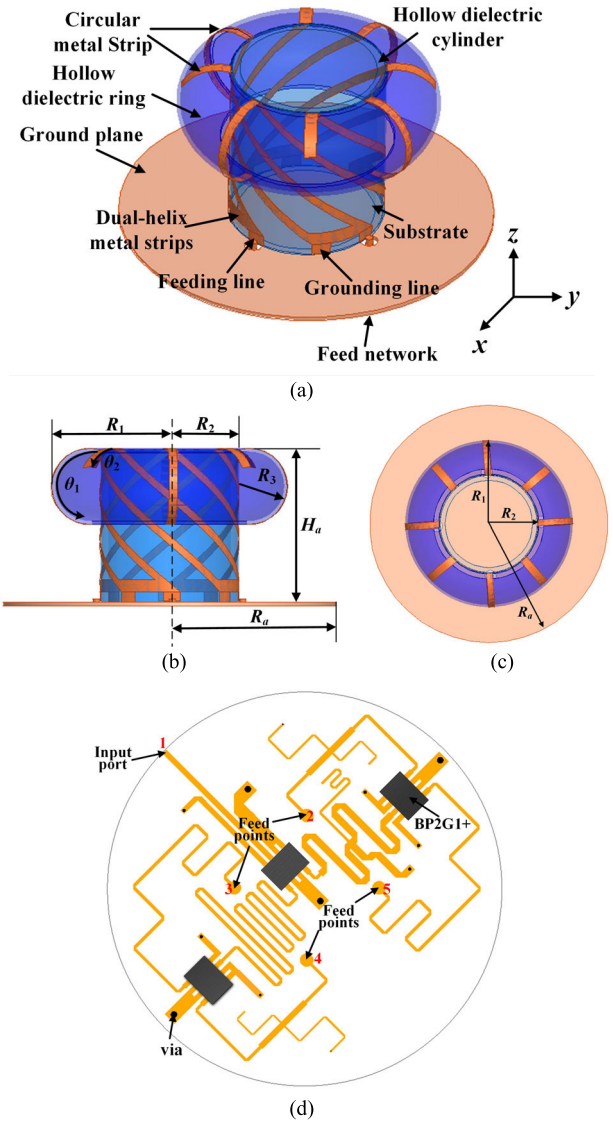

FIGURE 1. Structure of the proposed PQHA. (a) Perspective view. (b) Side view. (c) Top view. (d) Feed network.

shifters with shortened stubs are also proposed for further miniaturization.

Figure 2 shows the expanded view of one pair of the radiation elements. The arms in Part I are the dual-helix metal strips etched on the external surface of the cylinder substrate. The arms in Part II are the circular metal strips supported by the hollow dielectric ring. By mounting the hollow dielectric ring on the top of the hollow dielectric cylinder, the arms in Part II are connected with the arms of Part I, resulting in the formation of two radiators. For dual-band GPS application, the longer arm is designed at 1.227 GHz and the shorter arm is designed at 1.575 GHz.

B. EVOLUTIONS OF THE PROPOSED PQHA

The evolutions of the proposed PQHA are shown in Figure 3. Firstly, a traditional PQHA resonated at 1.575 GHz

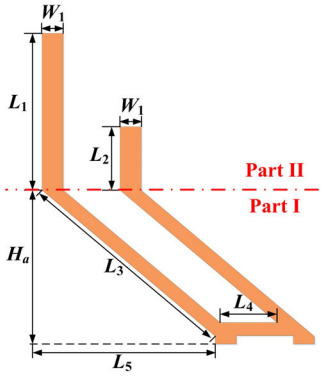

FIGURE 2. Expanded view of one pair of the arms.

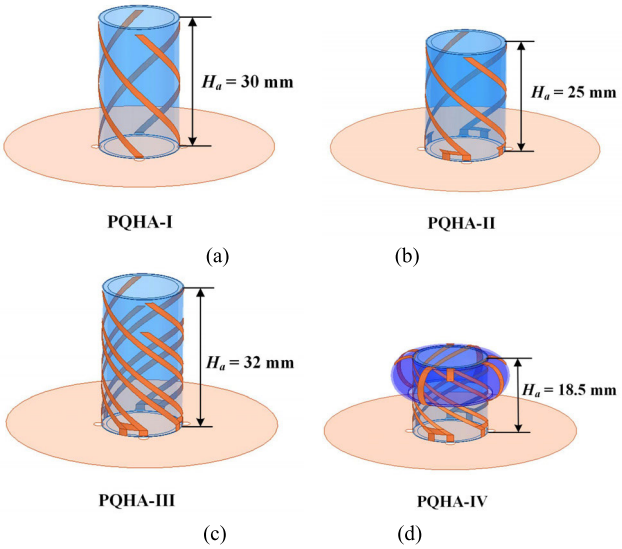

FIGURE 3. The evolutions of the proposed PQHA.

is designed, as shown in Figure 3(a) (named as PQHA-I). Each helix arm is designed to be λ/4 and 1/2 turn. As a result, the width (w_1) and length ($l_2+ l_3$) of the arm are optimized as 1.6 mm and 40 mm, respectively, with a radius (R_2) of 10 mm. The overall height of the dielectric cylinder (H_a) is 30 mm. Figure 4 shows the simulated $|S_{11}|$ and a resonate frequency is observed at 1.575 GHz. However, the impedance matching is not good. To adjust the impedance, four grounding lines are added to each of the helix arm, as shown in Figure 3 (b) (named as PQHA-II). It can be seen from Figure 4 that the $|S_{11}|$ at 1.575 GHz is changed from −5.5 dB to −18 dB by inserting the grounding lines. For PQHA-II, the optimized overall height of the dielectric cylinder (H_a) is reduced to 25 mm with ($l_2+ l_3$) of 36.4 mm. The values of w_1 and R_2 are unchanged. Except of better impedance matching, size reduction is also obtained.

Next, another arm operating at 1.227 GHz is added for dual-band operation, as shown in Figure 3(c) (named as PQHA-III). By tuning the length ($l_1+ l_3$) of the added arm, dual-resonated frequencies can be observed, as shown in

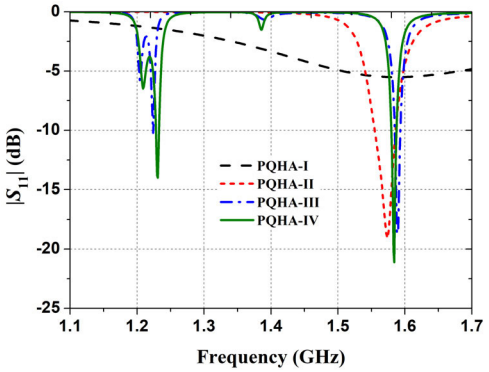

FIGURE 4. Simulated $|S_{11}|$ of the four evolution structures.

Figure 4. The optimized dimensions of ($l_1 + l_3$) are 45.5 mm, and the overall height of the dielectric cylinder (H_a) is increased to 32 mm. For further reducing the height of the dual-band antenna, the structure of Figure 3(d) is constructed (named as PQHA-IV). A hollow dielectric supporting ring is mounted on the top of the hollow dielectric supporting cylinder. By etching the circular metal strips on the dielectric ring, the height of the dielectric cylinder is reduced to 18.5 mm for resonating at the same two frequencies. Besides size reduction, wide 3-dB ARBW can also be obtained by using the circular metal strip. Figure 5 shows the simulated ARBW and half-power beamwidth (HPBW) of the four evolution structures at 1.575 GHz. It is observed that by using the circular metal strips, the 3-dB ARBW is enhanced while maintain the same HPBW.

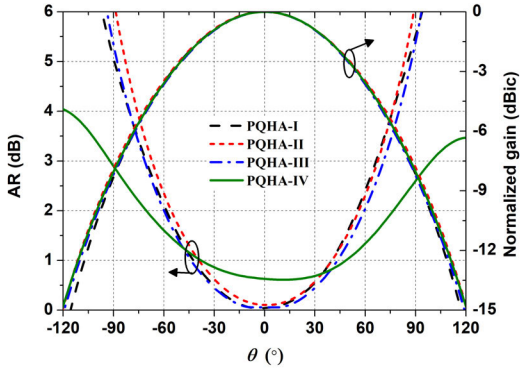

FIGURE 5. Simulated beamwidth of the four evolutions at 1.575 GHz.

C. PARAMETRIC STUDY OF THE PROPOSED PQHA

Since our design makes use of the circular metal strips to reduce height and enhance the 3-dB ARBW, a parametric study is presented in this section to illustrate the effects. Firstly, the radius of the circular metal strip is investigated. Figure 6 shows the different cases of the circular metal strips. Since the length of the circular metal strip directly affects the resonant frequency, the arm radius R_3 and the subtended angles (θ_1 and θ_2) in each case are chosen in such a way

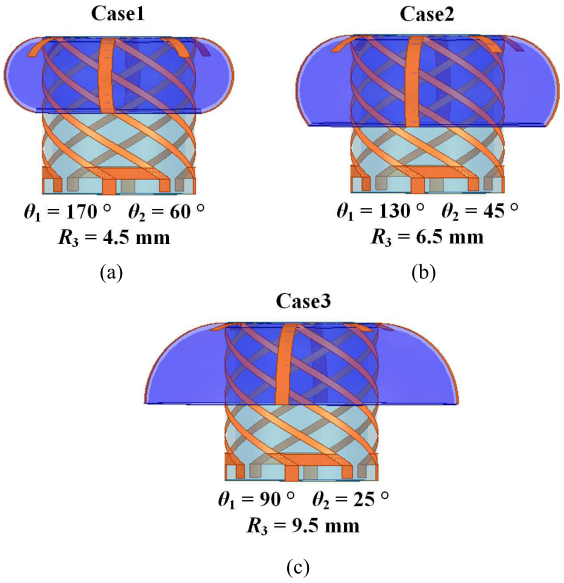

FIGURE 6. Different cases of the circular metal strip. (a) Case1. (b) Case2. (c) Case3.

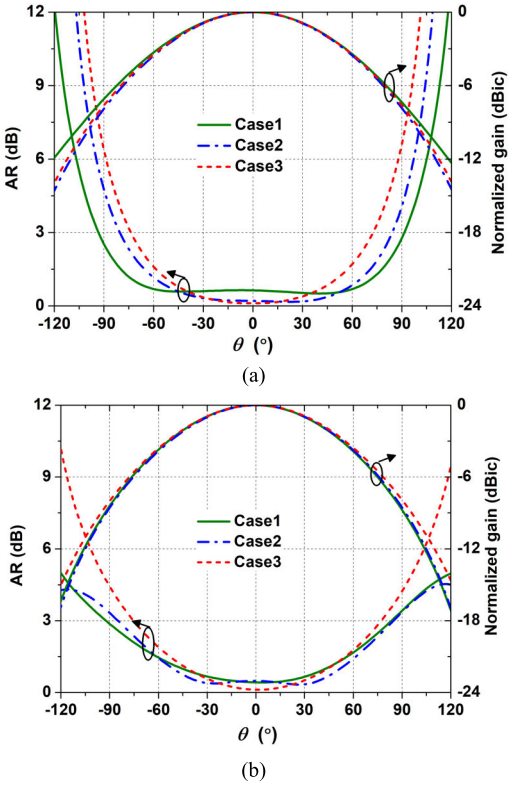

FIGURE 7. Simulated ARBWs and HPBWs of the three cases. (a) 1.227 GHz. (b) 1.575 GHz.

that all of the different cases resonate at 1.575 GHz and 1.227 GHz. The optimized values of the arm radius R_3 and the subtended angles (θ_1 and θ_2) for each case are also provided in Figure 6. It is observed that to resonate at the same frequency, the values of θ_1 and θ_2 are decreased with the increasing of R_3.

Figure 7 shows the simulated gain and AR in the $\varphi = 0°$ elevation plane for the different cases. It is observed that with the increase of θ_1 and θ_2, the 3-dB ARBW at the two resonate frequencies are both enhanced. While the changing of the HPBWs are not obvious. In detail, at 1.227 GHz, the 3-dB ARBW for $\theta_1 = 90°$, 130°, and 170° are given by 146°, 164° and 186°, respectively. And the values of HPBW are 114°, 110°, and 112°. At 1.575 GHz, the 3-dB ARBW for $\theta_1 = 90°$, 130°, and 170° are 152°, 169° and 176°, respectively. The values of HPBW for the three cases are all 108°. Thus, larger values of θ_1 and θ_2 are preferred for wide 3-dB ARBW. However, it should be mentioned that θ_1 can't be larger than 180° for avoiding the connection with the dual-helix metal strip.

Secondly, the influence of the distance between the dual-helix metal strip (named as the connecting line L_4) is discussed. Since the connecting line (L_4) is etched on a cylinder, the rotated angle θ_3 of the connecting line is utilized as the variable. Figure 8 shows the simulated ARBWs of the PQHA when the value of θ_3 is varied in the range of 35° to 55°. The corresponding values of L_4 are also provided. It is observed from Figure 8(a) that the 3-dB ARBW is nearly constant at 1.227 GHz, which indicates that the distance between the dual-helix metal strips shows less influence on the ARBW at GPS L2 band. While it is found from Figure 8(b) that the 3-dB ARBW at 1.575 GHz is slightly changed with the distance. Widest 3-dB ARBW is obtained at $\theta_3 = 45°$. When θ_3 is less than or larger than 45°, the arm resonated at 1.575 GHz is more closed to the arm resonated at 1.227 GHz. Since small distance enhances the mutual coupling, the radiation at 1.575 GHz will be affected by the adjacent radiation arm. Finally, the value of θ_3 is chosen as 45°, and the corresponding value of L_4 is 5.5 mm. Other parameters are optimized using the HFSS, and the optimal dimensions of the PQHA are listed in Table 1.

TABLE 1. Dimensions of the proposed PQHA (mm).

R_1	R_2	R_3	θ_1	θ_2	H_a	R_a
13.5	9	4.5	170	60	18.5	30
W_1	L_1	L_2	L_3	L_4	L_5	
1.6	13.3	4.4	32.8	5.5	31.4	

D. DESIGN OF THE MINIATURIZED FEED NETWORK

In order to provide equal amplitude signals with sequentially phases of 0°, −90°, −180°, and −270°, a quad-feed network is designed, as shown in Figure 1(d). It is composed of three Wilkinson power dividers, a 180° phase shifter, and two 90° phase shifters. For UAV Application, the dimensions of the feed network should be as small as possible. Thus, methods of size reduction are applied. Firstly, the BP2G1+ chip working in the range of 1.2 GHz ∼ 2.0 GHz is utilized as the

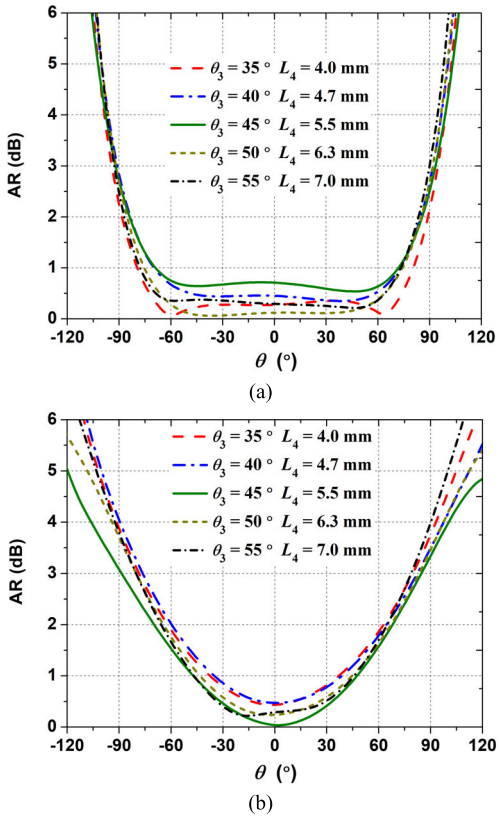

FIGURE 8. Simulated ARBWs with different values of θ_3. (a) 1.227 GHz. (b) 1.575 GHz.

power divider [21]. Secondly, a miniaturized wideband phase shifter is proposed to provide quadrature phases. In general, the topology in [22] is a simple one, which is composed of a main line and a reference line. The main line is realized by a combination of shunt λ/8 open-/short-ended stubs, while the reference line is a simple straight transmission line. However, the λ/8 open- /short-ended stubs are still large for limited design area. For further miniaturization, a modified structure of [22] is proposed, as shown in Figure 9.

The main line of the proposed phase shifter is composed of two transmission lines with characteristic impedance of Z_1 and electrical length of θ_1, an open-ended stub with characteristic impedance of Z_2 and electrical length of θ_2, and a short-ended stub with characteristic impedance of Z_3 and electrical length of θ_3. The reference line has a characteristic impedance of Z_4 and an electrical length of θ_4. In the following, the design formulas of the proposed phase shifter are

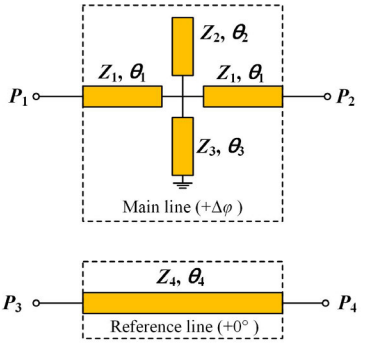

FIGURE 9. Schematic of the proposed phase shifter.

derived. Firstly, according to [23], the ABCD matrix of the reference line can be expressed by

$$[A]_R = \begin{bmatrix} \cos\theta_4 & \mathrm{j}Z_4 \sin\theta_4 \\ \dfrac{\mathrm{j}\sin\theta_4}{Z_4} & \cos\theta_4 \end{bmatrix} \tag{1}$$

While, the ABCD matrix of the main line is (2a) and (2b), as shown at the bottom of the page.

By converting the ABCD matrices into the scattering matrices, the transmission phase shift of the main line is calculated to be

$$\angle S_{p21} = -\arctan\left[\frac{2Z_1\left(Z_1 a_1 \sin^2\theta_1 - \sin 2\theta_1\right)}{Z_0\left(2\cos 2\theta_1 - Z_1 a_1 \sin 2\theta_1\right)}\right] \tag{3}$$

and that of the reference line is

$$\angle S_{p43} = -\theta_4 \tag{4}$$

Therefore, the transmission phase difference of the two paths is

$$\Delta\varphi = \theta_4 - \arctan\left[\frac{2Z_1\left(Z_1 a_1 \sin^2\theta_1 - \sin 2\theta_1\right)}{Z_0\left(2\cos 2\theta_1 - Z_1 a_1 \sin 2\theta_1\right)}\right] \tag{5}$$

To keep ideal impedance matching, the following relation should be satisfied, which is derived from $|S_{p11}| = 0$

$$a_1 = \frac{\sin 2\theta_1\left(Z_1^2 - Z_0^2\right)}{Z_1\left(Z_0^2\cos^2\theta_1 + Z_1^2\sin^2\theta_1\right)} \tag{6}$$

Then, substitute (6) into (5), derives (7), as shown at the bottom of the next page.

Using equations (2b), (6) and (7), the circuit parameters of the phase shifter can be obtained. The design procedures are listed below:

$$[A]_M = \begin{bmatrix} \cos 2\theta_1 - \dfrac{Z_1 \sin 2\theta_2}{2} a_1 & \mathrm{j}Z_1\left[\sin 2\theta_1 - Z_1 \sin^2\theta_1 a_1\right] \\ \dfrac{\mathrm{j}}{Z_1}\left[\sin 2\theta_1 + Z_1\cos^2\theta_1 a_1\right] & \cos 2\theta_1 - \dfrac{Z_1 \sin 2\theta_2}{2} a_1 \end{bmatrix} \tag{2a}$$

$$a_1 = \frac{\tan\theta_2}{Z_2} - \frac{\cot\theta_3}{Z_3} \tag{2b}$$

1) According to (7), the value of Z_1 can be calculated with predetermined θ_1, θ_4 and $\Delta\varphi$.
2) Under the condition of (2b) equals with (6), the values of θ_2, θ_3, Z_2 and Z_3 can be chosen arbitrarily.

Based on the above design procedure, the 90° phase shifter ($\Delta\varphi = 90°$) is firstly designed. The values of θ_1 and θ_4 are predetermined to be 12° and 100°, respectively. The value of Z_1 is calculated to be 20.6 Ω. Then the values of θ_2, θ_3, Z_2 and Z_3 can be chosen. When choosing, two limitations should be considered. First is the electrical length. Since the area of the feed network is limited, the electrical lengths of the open-/short- ended stubs should be as short as possible. Second is the characteristic impedance. High impedance should not to be chosen for avoiding high fabrication difficulties. Finally, the values of θ_2, θ_3, Z_2 and Z_3 are chosen as 25°, 31°, 70 Ω, and 70 Ω, respectively. For the 180° phase shifter ($\Delta\varphi = 180°$), the values of θ_1 and θ_4 are predetermined to be 73° and 280°, respectively. The value of Z_1 is calculated to be 18.2 Ω. The values of θ_2, θ_3, Z_2 and Z_3 are chosen as 19°, 28°, 62 Ω, and 14 Ω, respectively. Figure 10 shows the simulated results of the 90° and 180° phase shifters. The amplitude and phase characteristics in the desired frequency band are good enough for the feeding network design.

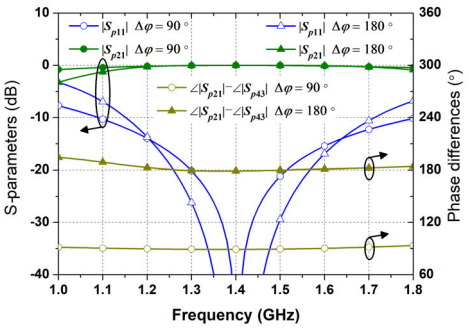

FIGURE 10. Simulated *S*-parameters and phase differences of the 90° and 180° phase shifters.

III. FABRICATION AND MEASUREMENTS

The fabricated photograph of the proposed PQHA is shown in Figure 11. The performance of the fabricated PQHA is measured by PNA network analyzer N5230A and anechoic chamber. Figure 12 shows the measured $|S_{11}|$ of the fabricated PQHA integrated with the feed network. It is seen that the measured $|S_{11}|$ is less than -10 dB in the range of $1.1 \sim 1.65$ GHz. The measured AR and peak gain versus the frequency are shown in Figure 13. It is observed that the AR is less than 3 dB in the ranges of 1.15 GHz $\sim$ 1.30 GHz and 1.52 GHz $\sim$ 1.60 GHz. At 1.227 GHz, the measured

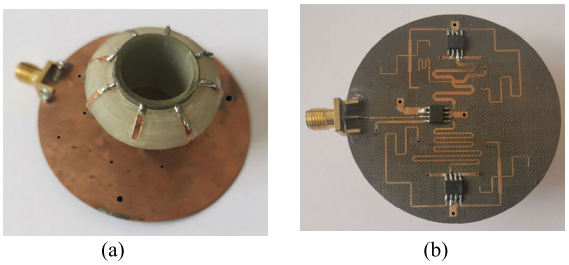

FIGURE 11. Photograph of the fabricated PQHA. (a) 3D view. (b) Feed network.

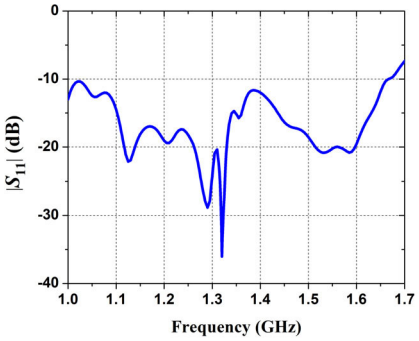

FIGURE 12. Measured $|S_{11}|$ of the fabricated PQHA.

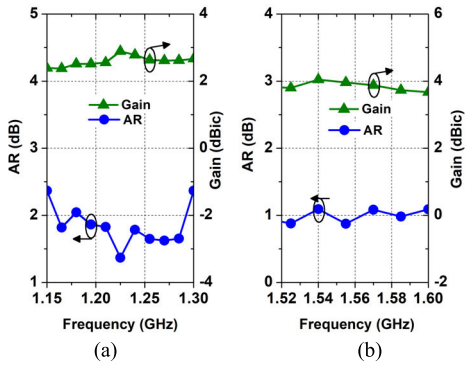

FIGURE 13. Measured AR and gain of the fabricated PQHA. (a) L2 band. (b) L1 band.

gain is 2.9 dBic, and the value is 3.9 dBic at 1.575 GHz. Figure 14 shows the measured radiation efficiency of the fabricated PQHA. It is observed that from 1.15 GHz to 1.3 GHz, the radiation efficiency is more than 60 %, while from 1.52 GHz to 1.6 GHz, the values are more than 80 %. At 1.227 GHz and 1.575 GHz, the efficiencies are 75.8 % and 89.6 %, respectively.

In Figure 15, the measured radiation patterns compared to the simulated ones are shown for GPS L2 (1.227 GHz)

$$\Delta\varphi = \theta_4 - \arctan\left[\frac{2Z_1Z_0\sin 2\theta_1}{Z_0^2\left(2\cos 2\theta_1\cos\theta_1^2 + \sin^2 2\theta_1\right) + Z_1^2\left(2\cos 2\theta_1\sin\theta_1^2 - \sin^2 2\theta_1\right)}\right] \tag{7}$$

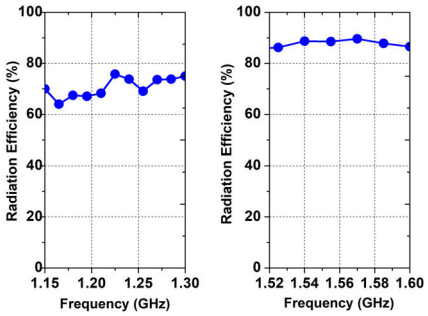

FIGURE 14. Measured radiation efficiency of the fabricated PQHA.

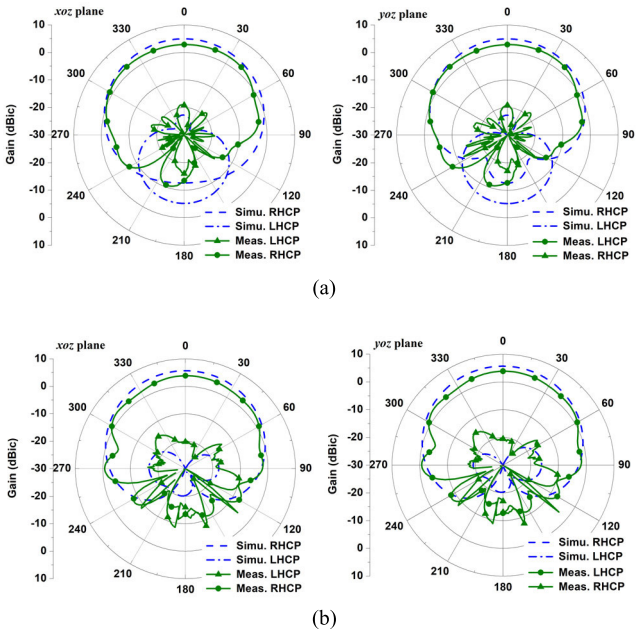

FIGURE 15. Simulated and measured radiation patterns. (a) 1.227 GHz. (b) 1.575 GHz.

and L1 (1.575 GHz) band. It is observed that the patterns in the *xoz* and *yoz* planes are similar to each other and the radiation patterns of RHCP is symmetric for the maximum radiation direction. The co-polar (RHCP) field is stronger than the cross-polar (LHCP) counterpart by at least 16 dB over a wide range of elevation angle θ, giving a wide 3-dB ARBW. At 1.227 GHz, the measured HPBW are 128° and 126° for *xoz* and *yoz* planes, respectively. While the values are 122° and 120° at 1.575 GHz. Figure 16 shows the simulated and measured ARs of the proposed antenna at the *xoz* and *yoz* planes. The measured 3-dB ARBWs are 186° and 187° at 1.277 GHz, respectively. While at 1.575 GHz, the corresponding values are 167° and 163°.

Table 2 shows the comparisons between the proposed and previous reported PQHAs. It is observed that by loading the circular metal strips, the proposed antenna shows the lowest height. Besides, wide 3-dB ARBW is also obtained which is usually ignored by other researches. Based on the advantages of low profile and wide beamwidth, the proposed antenna can be a good candidate for UAV GPS applications.

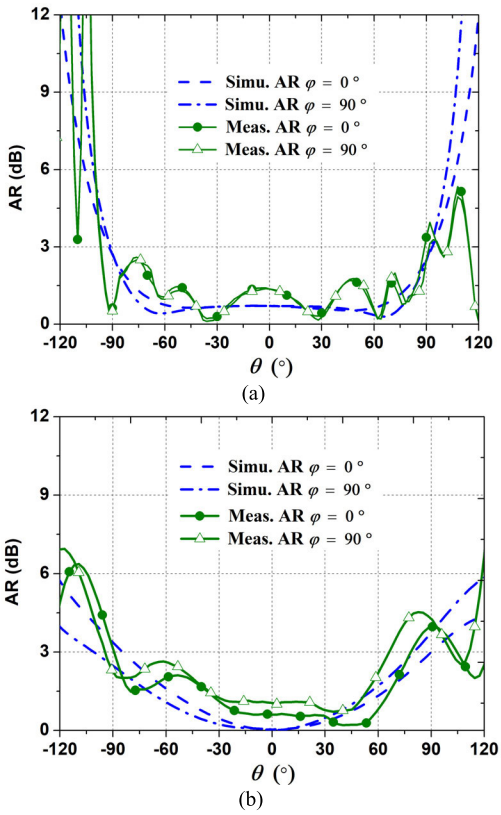

FIGURE 16. Simulated and measured AR. (a) 1.227 GHz. (b) 1.575 GHz.

TABLE 2. Comparisons between the proposed and previous reported PQHAs.

Ref.	Freq. (GHz)	Height (λ_0)	Diameter (λ_0)	3-dB ARBW (°)	HPBW (°)
[17]	1.227/1.575	0.33	0.18	N/A	80/73.6
[18]	1.227/1.575	0.35	0.12	N/A	96/122
[19]	1.14/1.54 /1.84	0.30	0.15	N/A	126/156 /172
[20]	1.227/1.575	0.1	0.05	N/A	N/A
This work	**1.227/1.575**	**0.07**	**0.11**	**186/163**	**126/120**

λ_0 is the free space wavelength at 1.227 GHz.

IV. CONCLUSION

In the paper, the design of a low-profile dual-band PQHA with wide beamwidth is presented. The dual-band operation is realized by using the dual-helix metal strips with different lengths. The height of the proposed PQHA is shortened by using the circular metal strips. Moreover, wide beamwidth is also obtained. To provide equal amplitude signals with sequentially quadrature phases, a miniaturized quad-feed network is designed, which is composed of the chip-based power divider and the proposed modified phase shifter. To validate, a prototype working at GPS L1/L2 bands is designed, fabricated and measured. The height of the fabricated PQHA is $0.07\lambda_0$. At 1.227 GHz, the measured 3-dB ARBW and

HPBW are 186°/187° and 128°/126°, respectively. While the values are 167°/163° and 122°/120° at 1.575 GHz. The results validate the design methods and suggest that the proposed antenna can be a good candidate for UAV applications.

REFERENCES

[1] J.-M. Fernandez Gonzalez, P. Padilla, J. F. Valenzuela-Valdes, J.-L. Padilla, and M. Sierra-Perez, "An embedded lightweight folded printed quadrifilar helix antenna: UAV telemetry and remote control systems," *IEEE Antennas Propag. Mag.*, vol. 59, no. 3, pp. 69–76, Jun. 2017.
[2] Y. Chen and C.-F. Wang, "Electrically small UAV antenna design using characteristic modes," *IEEE Trans. Antennas Propag.*, vol. 62, no. 2, pp. 535–545, Feb. 2014.
[3] X. Bai, J. Tang, X. Liang, J. Geng, and R. Jin, "Compact design of triple-band circularly polarized quadrifilar helix antennas," *IEEE Antennas Wireless Propag. Lett.*, vol. 13, pp. 380–383, 2014.
[4] Q.-X. Chu, W. Lin, W.-X. Lin, and Z.-K. Pan, "Assembled dual-band broadband quadrifilar helix antennas with compact power divider networks for CNSS application," *IEEE Trans. Antennas Propag.*, vol. 61, no. 2, pp. 516–523, Feb. 2013.
[5] J. Costantine, Y. Tawk, I. Maqueda, M. Sakovsky, G. Olson, S. Pellegrino, and C. G. Christodoulou, "UHF deployable helical antennas for CubeSats," *IEEE Trans. Antennas Propag.*, vol. 64, no. 9, pp. 3752–3759, Sep. 2016.
[6] C. C. Kilgus, "Resonant quadrifilar helix," *IEEE Trans. Antennas Propag.*, vol. AP-17, no. 3, pp. 349–351, May 1969.
[7] Y. Letestu and A. Sharaiha, "Broadband folded printed quadrifilar helical antenna," *IEEE Trans. Antennas Propag.*, vol. 54, no. 5, pp. 1600–1604, May 2006.
[8] S. Hebib, N. J. G. Fonseca, and H. Aubert, "Compact printed quadrifilar helical antenna with Iso-Flux-Shaped pattern and high cross-polarization discrimination," *IEEE Antennas Wireless Propag. Lett.*, vol. 10, pp. 635–638, 2011.
[9] Y.-S. Wang and S.-J. Chung, "A miniature quadrifilar helix antenna for global positioning satellite reception," *IEEE Trans. Antennas Propag.*, vol. 57, no. 12, pp. 3746–3751, Dec. 2009.
[10] Z.-Y. Zhang, L. Yang, S.-L. Zuo, M. U. Rehman, G. Fu, and C. Zhou, "Printed quadrifilar helix antenna with enhanced bandwidth," *IET Microw., Antennas Propag.*, vol. 11, no. 5, pp. 732–736, Apr. 2017.
[11] B. Desplanches, A. Sharaiha, and C. Terret, "Parametrical study of printed quadrifilar helical antennas with central dielectric rods," *Microw. Opt. Technol. Lett.*, vol. 20, no. 4, pp. 249–255, Feb. 1999.
[12] Y. Tawk, M. Chahoud, M. Fadous, J. Costantine, and C. G. Christodoulou, "The miniaturization of a partially 3-D printed quadrifilar helix antenna," *IEEE Trans. Antennas Propag.*, vol. 65, no. 10, pp. 5043–5051, Oct. 2017.
[13] M. Amin and R. Cahill, "Effect of helix turn angle on the performance of a half wavelength quadrifilar antenna," *IEEE Microw. Wireless Compon. Lett.*, vol. 16, no. 6, pp. 384–386, Jun. 2006.
[14] D. K. C. Chew and S. R. Saunders, "Meander line technique for size reduction of quadrifilar helix antenna," *IEEE Antennas Wireless Propag. Lett.*, vol. 1, pp. 109–111, 2002.
[15] X.-F. Wang, X.-J. Li, H. Wang, and S.-G. Zhou, "Design of a compact and wideband quadrifilar helix antenna," in *Proc. IEEE Asia–Pacific Conf. Antennas Propag. (APCAP)*, Auckland, New Zealand, Aug. 2018, pp. 68–69.
[16] W. Qin, L.-H. Shi, W.-J. Sun, W.-W. Yang, L. Ge, and J.-X. Chen, "A wideband LTCC quad-phase power dividing network and its application to ceramic-based quadrifilar helix antennas," *IEEE Access*, vol. 7, pp. 141094–141103, 2019.
[17] G. Byun, H. Choo, and S. Kim, "Design of a dual-band quadrifilar helix antenna using stepped-width arms," *IEEE Trans. Antennas Propag.*, vol. 63, no. 4, pp. 1858–1862, Apr. 2015.
[18] Y.-H. Yang, J.-L. Guo, B.-H. Sun, and Y.-H. Huang, "Dual-band slot helix antenna for global positioning satellite applications," *IEEE Trans. Antennas Propag.*, vol. 64, no. 12, pp. 5146–5152, Dec. 2016.
[19] J. Rabemanantsoa and A. Sharaiha, "Size reduced multi-band printed quadrifilar helical antenna," *IEEE Trans. Antennas Propag.*, vol. 59, no. 9, pp. 3138–3143, Sep. 2011.
[20] Y. Han, H. Wang, Z. Wang, Y. Yao, Y. Feng, K. Hu, Y. Gao, Z. Fan, and S. Yuan, "Dual-band spiral printed quadrifilar helical antenna miniaturized by surface and inner dielectric loading," *IEEE Access*, vol. 7, pp. 30244–30251, 2019.
[21] *Data Sheet-BP2G1*. Accessed: Jul. 26, 2020. [Online]. Available: https://www.alldatasheet.com/datasheet-pdf/pdf/1005773/MINI/BP2G1.html
[22] S. Y. Zheng, S. H. Yeung, W. S. Chan, K. F. Man, and S. H. Leung, "Improved broadband dumb-bell-shaped phase shifter using multi-section stubs," *IET Electron. Lett.*, vol. 44, no. 7, pp. 478–480, Mar. 2008.
[23] D. M. Pozar, *Microwave Engineering*, 4th ed. Hoboken, NJ, USA: Wiley, 2012.

HONGMEI LIU (Member, IEEE) received the Ph.D. degree in information and communication engineering from Dalian Maritime University (DMU), Liaoning, China, in 2016. She is currently an Associate Professor with the School of Information Science and Technology, DMU. Her current research interests include CP microwave antennas, passive microwave circuits, and reconfigurable RF components. She is currently serving as a Technical Reviewer for the IEEE TRANSACTIONS ON INDUSTRIAL ELECTRONICS, the *Electronics Letters*, and the *International Journal of RF and Microwave Computer-Aided Engineering*. She was a recipient of the Best Doctor's Dissertation Award of Liaoning Province in 2017.

MINGKE SHI was born in Yunnan, China. He received the master's degree in electronic science and technology from Dalian Maritime University (DMU). He is currently an Electrical Engineer with the Kunming Shipborne Equipment Research and Test Center, China State Shipbuilding Corporation Ltd. His research interests include helix antennas, GPS antennas, and phase shifters.

SHAOJUN FANG (Member, IEEE) received the Ph.D. degree in communication and information systems from Dalian Maritime University (DMU), Liaoning, China, in 2001. Since 1982, he has been with the DMU, where he is currently the Head Professor with the School of Information Science and Technology. He has authored or coauthored three books and over 100 journal articles and conference papers. His recent research interests include passive RF components, patch antennas, and computational electromagnetics. He was a recipient of the Best Doctor's Dissertation Award of Liaoning Province in 2002 and the Outstanding Teacher Award of the Ministry of Transport of China.

ZHONGBAO WANG (Member, IEEE) received the Ph.D. degree in communication and information systems from Dalian Maritime University (DMU), Liaoning, China, in 2012. He is currently an Associate Professor with the School of Information Science and Technology, DMU. He has authored or coauthored over 60 papers in journals and conferences. His current research interests include passive RF components, patch antennas, and microwave technology using artificial intelligence. He is currently serving as a Technical Reviewer for the IEEE TRANSACTIONS ON MICROWAVE THEORY AND TECHNIQUES, the IEEE ANTENNAS AND WIRELESS PROPAGATION LETTERS, IEEE Access, the *IET Microwaves, Antennas, and Propagation*, *Electronics Letters*, the *Electronics and Telecommunications Research Institute (ETRI) Journal*, *Radioengineering*, and the *International Journal of RF and Microwave Computer-Aided Engineering*. He was a recipient of the Best Doctor's Dissertation Award of Liaoning Province in 2013.